

Article

Catalyst Coatings for Ammonia Decomposition in Microchannels at High Temperature and Elevated Pressure for Use in Decentralized and Mobile Hydrogen Generation

Tobias Weissenberger ^{*}, Ralf Zapf, Helmut Pennemann and Gunther Kolb 

Fraunhofer Institute for Microengineering and Microsystems IMM, Carl-Zeiss-Straße 18-20, 55129 Mainz, Germany; gunther.kolb@imm.fraunhofer.de (G.K.)

^{*} Correspondence: tobias.weissenberger@imm.fraunhofer.de

Abstract: We report an investigation of catalyst performance for the decomposition of ammonia under industrially relevant conditions (high temperatures of up to 800 °C and an elevated pressure of 5 bar) with further emphasis on their stability at high reaction temperatures. The catalysts were applied and tested as coatings in 500 µm wide channels of microreactors. Nickel-based catalysts were studied and compared to a ruthenium-based catalyst supported on SiO₂. The effect of the support on the catalytic performance was investigated, and CeO₂-supported nickel catalysts were found to exhibit the highest activity. Promoters were applied to increase the NH₃ decomposition activity of the Ni/CeO₂ catalysts. The addition of cesium led to a slight reduction in activity, while lanthanum, calcium, and barium doping resulted in increased activity. In particular, the barium-doped Ni/CeO₂ catalyst showed very high ammonia conversion and closed the activity gap with respect to ruthenium catalysts at reactor temperatures of 650 °C and higher. The hydrogen production rates achieved in this work were compared to values in the literature and were shown to exceed values found earlier for both nickel- and ruthenium-based catalysts. Furthermore, the ruthenium-based catalysts under investigation were rapidly deactivated at 700 °C, while the nickel-based catalysts did not show deactivation after 220 h on time on stream at 700 °C.



Citation: Weissenberger, T.; Zapf, R.; Pennemann, H.; Kolb, G. Catalyst Coatings for Ammonia Decomposition in Microchannels at High Temperature and Elevated Pressure for Use in Decentralized and Mobile Hydrogen Generation. *Catalysts* **2024**, *14*, 104. <https://doi.org/10.3390/catal14020104>

Academic Editors: Hugo de Lasa and Mohammad Mozahar Hossain

Received: 16 November 2023

Revised: 11 January 2024

Accepted: 19 January 2024

Published: 26 January 2024



Copyright: © 2024 by the authors. Licensee MDPI, Basel, Switzerland. This article is an open access article distributed under the terms and conditions of the Creative Commons Attribution (CC BY) license (<https://creativecommons.org/licenses/by/4.0/>).

Keywords: ammonia; hydrogen; ammonia decomposition; fuel cells; hydrogen carrier; energy carrier

1. Introduction

Hydrogen (H₂) is widely considered to have the potential to become a major green energy vector [1]. However, the storage and transport of hydrogen are major challenges [2]. Hydrogen possesses the lowest density among all elements, resulting in a very poor energy density of only 3 Wh per liter. Therefore, for storage and transportation, hydrogen must be compressed to a high pressure (up to 700 bar) or liquefied to a cryogenic temperature of −253 °C. But even in its liquid form, the energy density of hydrogen is comparably low due to its low liquid density of only 75 kg/m³.

Ammonia is emerging as a hydrogen carrier due to its high hydrogen storage density of 17.7 wt.%, high energy density of 3 kWh/kg_{NH₃}, and the fact that it can be liquefied at a moderate pressure of only 0.86 MPa at 20 °C. Hydrogen then can be generated through the decomposition of carbon-free ammonia into hydrogen and nitrogen. The synthesis of ammonia consumes less than 10% of the energy required to produce hydrogen through water electrolysis [3].

Approximately 150 Mt of ammonia is produced worldwide each year [4]. Technologies for the synthesis, storage, and transportation of ammonia are well established and widely available. However, the technology for hydrogen generation through ammonia decomposition and subsequent hydrogen purification is not as advanced. Thus, the development of advanced catalysts and efficient reactor technology for ammonia decomposition is required for the future application of ammonia as a hydrogen carrier [4].

Decentralized ammonia decomposition units can provide hydrogen at facilities that are not connected to the hydrogen infrastructure, e.g., for hydrogen fueling stations, use in chemical processes, or in energy or heat generation via fuel cells or direct combustion. Other applications for small decomposition units include mobile applications, for example, in the automotive or maritime sector [5].

Many applications make the operation of the decomposition catalyst at an elevated pressure necessary. For example, if the produced hydrogen will be purified through pressure swing adsorption or via membrane separation, a pressure of 10 bar is required. To increase the pressure by an additional compressor downstream of the decomposition reactor causes several disadvantages.

Another example is a process of partial splitting of ammonia to utilize a hydrogen–ammonia mixture in an internal combustion engine, where the injection pressure may also be about 10 bar.

Operating a decomposition reactor at elevated pressure has many practical advantages but unfortunately shifts the chemical equilibrium towards ammonia, hence reducing the obtainable conversion level. To shift the chemical equilibrium towards greater ammonia conversion, operation at higher temperatures is necessary. For example, at a reactor pressure of 5 bar, a temperature of over 600 °C is required to achieve an ammonia conversion rate exceeding 99% [6]. However, studies on ammonia decomposition found in the literature were almost exclusively conducted at atmospheric pressure. Only a few studies at elevated pressure can be found [7–9].

Various metals are active in ammonia decomposition. Studies have outlined that the activity of different metals follows the order $Ru > Ni > Rh > Co > Ir > Fe$ [10]. Therefore, the most commonly applied catalysts for ammonia decomposition are based on ruthenium (Ru) and nickel (Ni).

Ruthenium exhibits the highest activity for ammonia decomposition [11]. Many different supports have been studied, including carbon nanotubes (CNTs), Pr_6O_{11} , CeO_2 , TiO_2 , Al_2O_3 , MgO , perovskites, fumed silica and mesoporous silica (MCM-41, SBA-15) [12–19]. Doping ruthenium catalysts with strong basic alkali, alkaline earth elements, and rare earth elements has resulted in enhanced performance [12,15,20–24]. The increase in efficiency is often attributed to the facilitation of nitrogen desorption due to electron transfer from the basic dopant to the ruthenium [11].

Ruthenium is very expensive, has a high global warming power (GWP), and might suffer from deactivation at elevated temperatures [25,26]. Nickel-based catalysts are cheaper than ruthenium and can reach good activities at higher temperatures. Additionally, there is much experience with nickel catalysts in high-temperature applications, such as methane steam reforming. Nickel-based catalysts are usually deposited on oxides such as silica [14], rare earth oxides [27,28], mixed oxides [29], zeolites [30], perovskites [31], and alumina [32], and carbon nanotubes have been used as support [33]. Promoters have been successfully applied to boost the ammonia decomposition activity of nickel and ruthenium catalysts. For example, alkali and alkaline earth metals have shown a promotive effect on the ammonia decomposition activity of ruthenium catalysts [11,34]. For nickel catalysts, the addition of rare earth oxides such as La_2O_3 and CeO_2 , as well as alkali and alkaline earth elements, significantly enhanced the ammonia decomposition activity [11,34–38].

We report the catalytic performance of nickel-based catalysts for ammonia decomposition under elevated pressures and high temperatures for use in microstructured reactors. Different supports were studied, and the loading of the active metal was varied. Additives were applied to increase the activity. Furthermore, the long-term stability of a selected catalyst was studied for 220 h.

The ammonia decomposition system for which the catalysts reported in the current study were developed consisted of a microstructured catalytic wall reactor with integrated heating through catalytic combustion, an evaporator and heat exchanger for heat recovery, and hydrogen purification through pressure swing adsorption. The plant was designed to produce hydrogen at 2.9 kg/h, which is sufficient to power a 50 kWh PEM fuel cell.

2. Results

2.1. Catalyst Characterization

Figure 1 shows a photograph of a catalyst-coated reactor plate with visible channels. The connection points for the inlet and outlet capillaries are visible on the left and right sides of the reactor. Two reactor plates were combined with the inlet and outlet capillaries and assembled by laser welding.



Figure 1. Photograph of a catalyst-coated reactor before assembly. The scale is in cm.

The surface areas of the different supports and catalysts are shown in Table 1. The specific surface areas of the supports ranged from $156 \text{ m}^2/\text{g}^{-1}$ for Al_2O_3 and over $103 \text{ m}^2/\text{g}^{-1}$ for SiO_2 to $37 \text{ m}^2/\text{g}^{-1}$ for CeO_2 . The corresponding catalysts showed a slight reduction in surface area compared to the pure supports due to the high density and low surface area of the nickel particles. The XRF analysis showed that the nickel loadings were in the range of 4.35 to 4.86% and were slightly lower than the set values of 5%. The loading of the additives barium, calcium, lanthanum, and cesium was very close to the loading of 1% set during catalyst preparation (see Table S1 in the Supplementary Materials).

Table 1. Characterization data for different nickel-based catalysts and pure catalyst supports.

Sample Loading in wt. %	Surface Area ¹ $\text{m}^2 \text{ g}^{-1}$	Metal Loading ² wt. %	Ni Dispersion ³ %	dp_{Ni} ⁴ nm
Al_2O_3	155.9	-	-	-
SiO_2	102.7	-	-	-
CeO_2	37.1	-	-	-
5% Ni/ Al_2O_3	147.5	4.86	7.98	12.7
5% Ni/ SiO_2	97.2	4.70	5.91	17.1
5% Ni/ CeO_2	33.7	4.67	4.29	23.5
10% Ni/ CeO_2	38.3	n.d.	4.13	24.3
15% Ni/ CeO_2	37.2	13.56	4.06	24.8
5% Ni, 1% Cs/ CeO_2	36.5	4.93	3.48	29.1
5% Ni, 1% La/ CeO_2	39.7	4.14	5.83	17.4
5% Ni, 1% Ba/ CeO_2	40.3	4.35	4.30	23.5

¹ BET (Brunauer–Emmett–Teller Method) surface area determined through N_2 sorption; ² metal loading measured with XRF; ³ nickel dispersion determined through H_2 chemisorption; ⁴ average particle diameters estimated with nickel dispersion assuming spherical particles.

The nickel particles were hard to distinguish from the supports in the TEM images shown in Figure 2. The Al_2O_3 support consisted of rod-like particles in different sizes. The SiO_2 support displayed spherical particles with diameters of about 40 nm, representing the particle size and shape of the colloidal silica. The CeO_2 support showed crystallites of different sizes and shapes.

Since the distribution of the nickel particles could not be determined using TEM, volumetric hydrogen chemisorption experiments were carried out. Table 1 lists the estimated nickel dispersions, nickel surface area, and particle sizes. The corresponding isotherms can be found in the Supplementary Materials. The data show that nickel supported on alumina

exhibited the highest dispersion of 7.98% and the smallest particles with an average diameter of 12.7 nm, followed by nickel supported on silica, which showed the second highest dispersion of 5.91%. The lowest dispersion of 4.29% was observed for nickel supported on CeO₂, resulting in an average particle diameter of 23.5 nm.

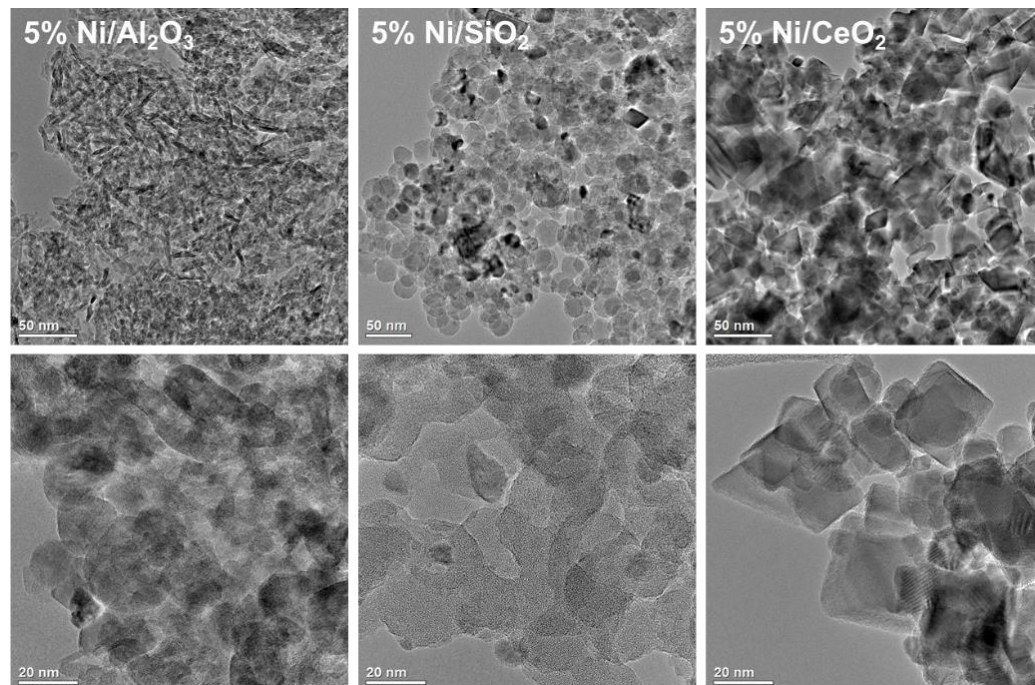


Figure 2. TEM micrographs of nickel-based catalysts supported on Al₂O₃, SiO₂, and CeO₂.

The catalysts with different nickel loadings showed a slight reduction in metal dispersion at higher loadings. The dispersion dropped from 4.29 to 4.06% for 5 and 15% nickel loadings, respectively. The addition of lanthanum (La) resulted in a small increase in dispersion to 5.8% from 4.3% for Ni/CeO₂. The addition of lanthanum during the catalyst preparation might have resulted in smaller nickel particles due to changes in pH or by altering the metal–support interactions. The addition of cesium (Cs) resulted in a reduction in the nickel dispersion (3.48%), indicating larger nickel particles. The addition of barium (Ba) showed no significant effects on the nickel dispersion compared to that of the Ni/CeO₂ catalyst without the addition of a promoter.

The EDX mappings of the cesium-, lanthanum-, and barium-doped Ni/CeO₂ samples are displayed in Figure 3. The mappings displayed an even distribution of the additives over the CeO₂ supports. Nickel was present in larger particles and was not as well dispersed as the additives. For both the cesium- and barium-doped catalysts, smaller and larger nickel particles were visible in the EDX mappings. The catalyst with lanthanum showed slightly smaller nickel particles and better dispersion of the particles compared to those of the barium- and cesium-doped catalysts, which was in good accordance with the H₂ chemisorption results.

The nickel-based catalysts on different supports were also investigated using X-ray photoelectron spectroscopy. The peaks were attributed to NiO and Ni(OH)₂ species according to the literature [39]. The data revealed that nickel was present as NiO and Ni(OH)₂ species in the calcined samples (see Figure 4). Differences could be measured in the fractions of NiO and Ni(OH)₂ in the different samples. The Ni/Al₂O₃ sample showed the largest fraction of Ni(OH)₂ species with 59.7%, followed by Ni/SiO₂ with 29.8% Ni(OH)₂. Ni/CeO₂ showed the smallest fraction of Ni(OH)₂ at 19.4%. This was also evident in the oxygen measurements (available in the Supplementary Materials), where a prominent Ni(OH)₂ peak was visible for the Al₂O₃ sample, and a less prominent peak was visible for the SiO₂ sample. The sample supported on CeO₂ did not show a Ni(OH)₂ peak there.

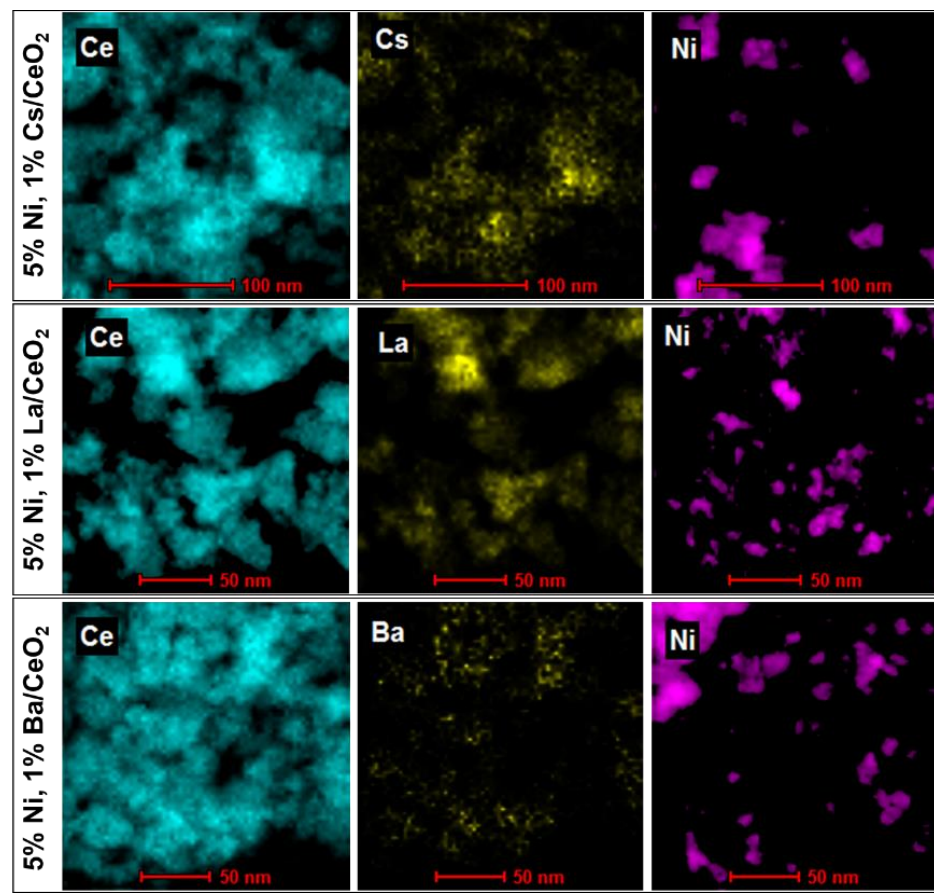


Figure 3. EDX mappings for Cs-, La-, and Ba-doped nickel catalysts supported on CeO₂.

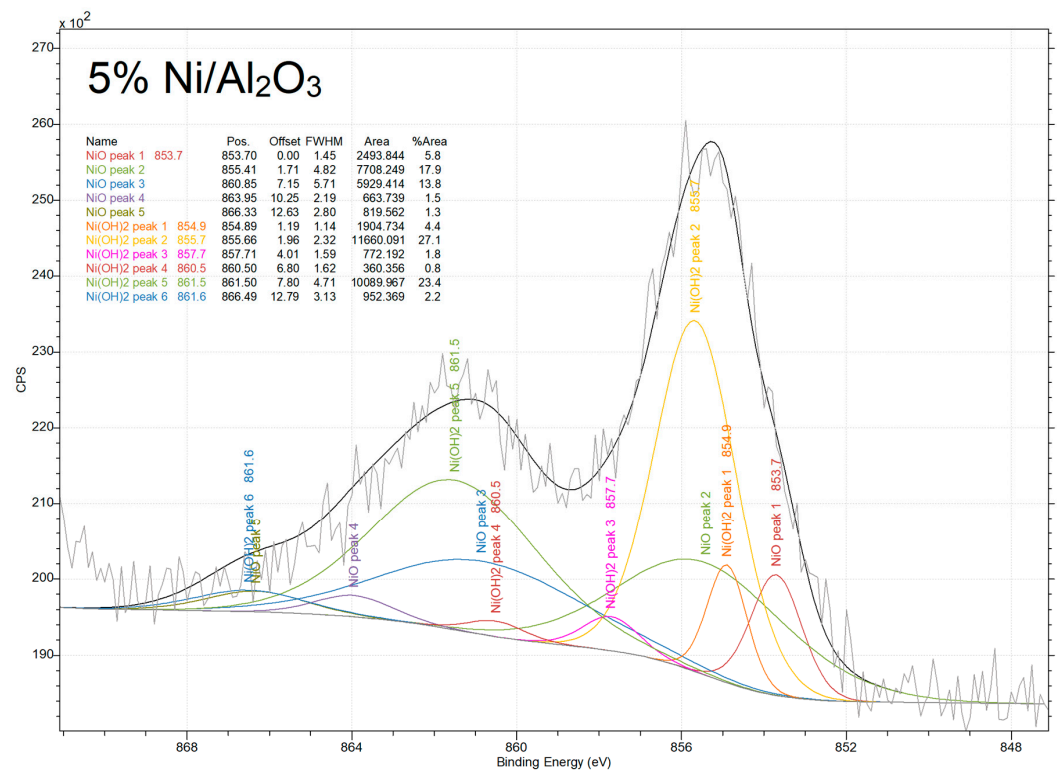


Figure 4. Cont.

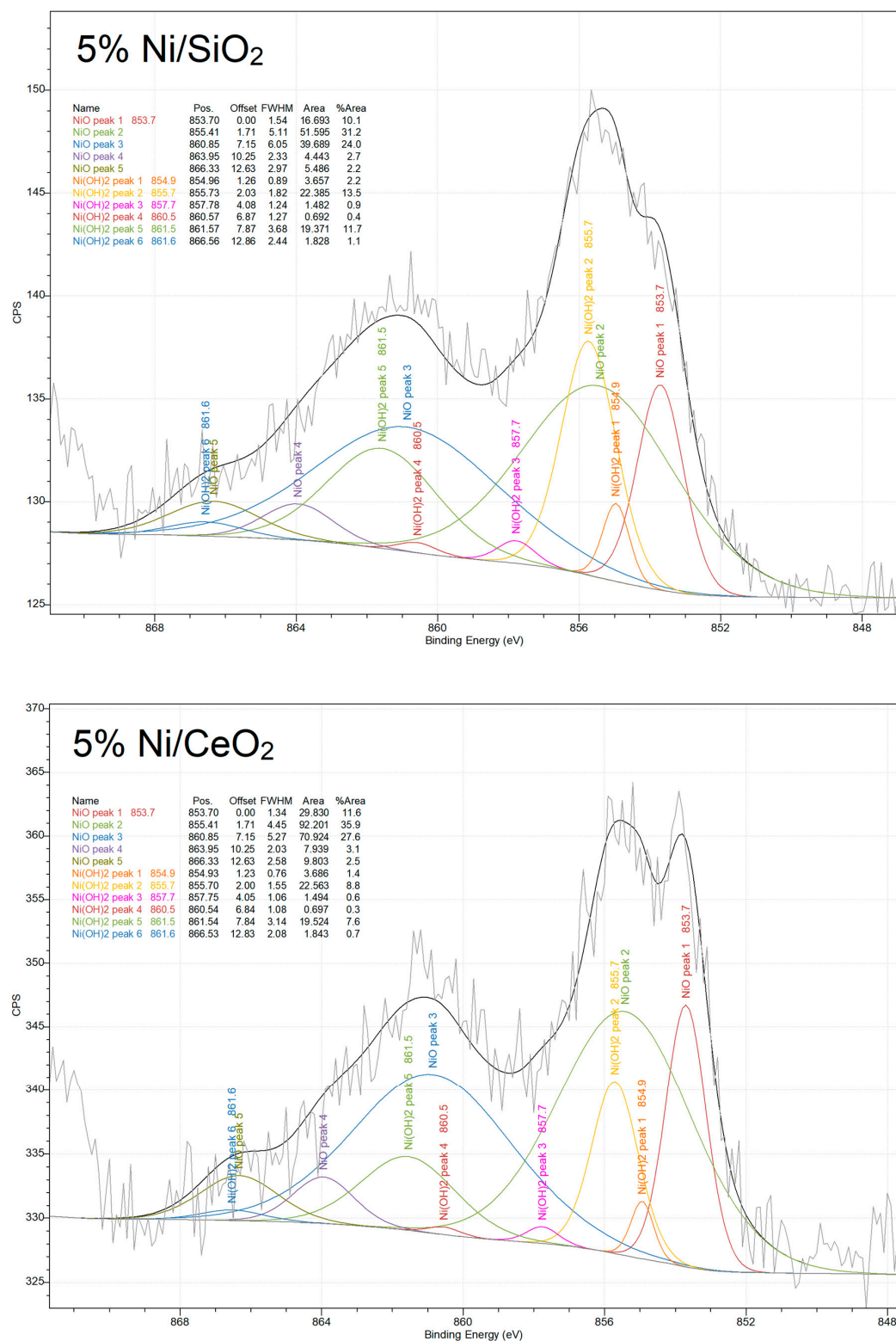


Figure 4. Results of curve fitting for XPS spectra (Ni_{2p}) for the nickel catalysts supported on different supports.

2.2. Catalytic Tests

2.2.1. Nickel Catalysts on Different Supports

The catalyst support played an important role, as was evident in the ammonia conversions shown in Figure 5. As a reference, a ruthenium catalyst supported on silica was chosen, since this support showed the best performance among the tested ruthenium

catalysts. Compared to the silica-supported ruthenium-based catalyst, the nickel catalysts showed lower activities, especially at lower temperatures. At higher reactor temperatures, the ammonia conversion increased, and the nickel-based catalysts reached similar conversion rates to that of the ruthenium-based catalyst. The nickel catalysts on different supports differed greatly in their degree of ammonia conversion. The aluminum-supported catalyst showed the lowest rate of ammonia conversion. The silica-supported catalyst showed a similarly low rate of conversion at lower temperatures. Only at temperatures of 700 °C and higher did the silica-supported catalyst surpass the aluminum-supported catalyst. The nickel catalyst supported on cerium dioxide showed much higher activity, especially at low temperatures. For example, at 650 °C, the nickel catalysts supported on silica and alumina reached around 20% ammonia conversion, while the ceria-supported catalyst reached 70% ammonia conversion. Generally, for the different supports, the order of activity was found to be $\text{CeO}_2 > \text{SiO}_2 > \text{Al}_2\text{O}_3$. Interestingly, the activity of the catalysts was inversely proportional to the dispersion of the nickel particles determined through H_2 chemisorption (see Table 1).

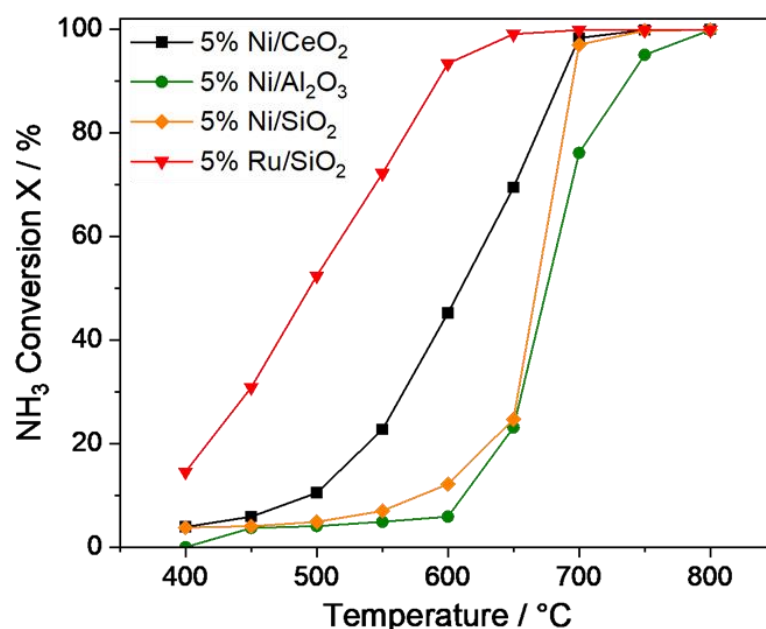


Figure 5. Ammonia conversion over reactor temperature for nickel catalysts on different supports (Ru/SiO₂ as a reference). WHSV = 200 L g_{cat}⁻¹ h⁻¹, 10% Ar, 90% NH₃, and *p* = 5 barg.

Since the activity did not correlate with the nickel particle size, other effects of the support likely caused the differences in activity. Further research is planned to gain insight into the mechanism behind the observed catalytic performance. In the literature, several possible explanations for the higher activity of the CeO₂-supported catalyst compared to the SiO₂- and Al₂O₃-supported catalysts are reported. Lucentini et al. also found that Ni/CeO₂ and Ru/CeO₂ catalysts were more active in ammonia decomposition than Ni/Al₂O₃ and Ru/Al₂O₃ were [40]. For nickel-based catalysts, they also observed a higher nickel dispersion for Al₂O₃-supported catalysts (average particle diameter of 3.3 nm) compared to that of a CeO₂-supported catalyst (average particle diameter of 5 nm), but they found a much higher activity for the CeO₂-supported catalyst. The difference in activity was attributed to a particular metal–support interaction.

CeO₂ is often used as a support or promoter for ammonia decomposition catalysts due to its large number of oxygen vacancies [41]. Do and coworkers found that CeO₂ showed effects on NiO reducibility, surface oxygen vacancies, basicity, and the nickel–support interaction [42]. A support with high basicity can donate electrons to nickel particles and, thus, lower the binding energy of nickel and nitrogen, which facilitates the associative desorption of nitrogen and results in enhanced activity in ammonia decomposition [42].

The morphology of the support can also change the activity of the catalyst. Chuanqing Huang and coworkers found that the activity of Ni/CeO₂ and Co/CeO₂ catalysts in ammonia decomposition was significantly altered by the morphology of the CeO₂ support [43].

2.2.2. Effect of the Nickel Loading

Since CeO₂ showed the best performance, the following investigations were carried out using the ceria support. The effect of the nickel loading on the degree of ammonia conversion can be seen in Figure 6. As expected, the ammonia conversion increased with increasing nickel loading. The biggest differences were observed for reaction temperatures in the range of 550 to 650 °C. At temperatures of 700 °C and higher, the differences between the nickel loadings became rather small.

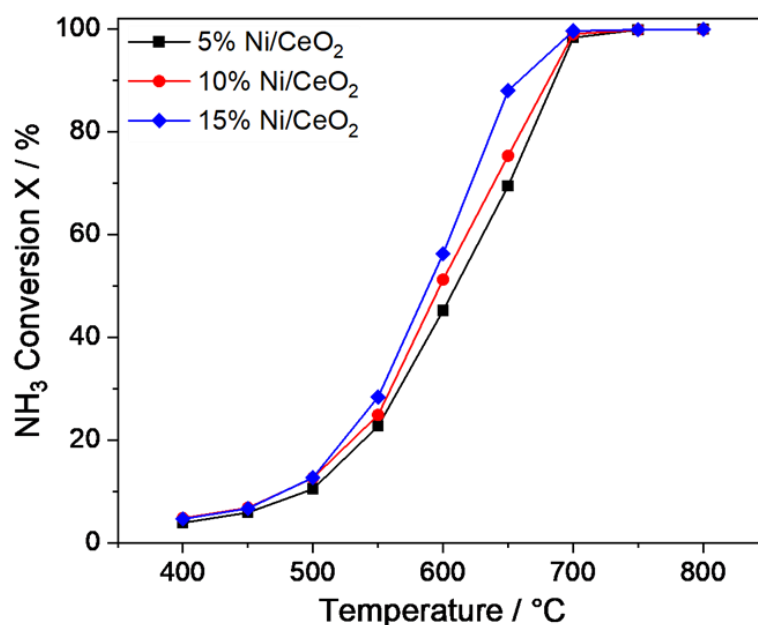


Figure 6. Ammonia conversion over reactor temperature for nickel catalysts supported on CeO₂ with different nickel loadings. WHSV = 200 L g_{cat}⁻¹ h⁻¹, 10% Ar, 90% NH₃, and *p* = 5 barg.

However, if one considers the significant increase in nickel loading, the gain in ammonia conversion was modest. As was evident in the H₂ chemisorption data, a higher loading resulted in slightly larger nickel particles and, thus, reduced metal dispersion. Nevertheless, the available nickel surface areas estimated through H₂ chemisorption increased from 1.43 m²/g_{cat} to 4.07 m²/g_{cat} with greater nickel loading. Thus, the reduced nickel dispersion could not fully explain the modest increase in activity of the catalysts.

2.2.3. Effects of Dopants on Nickel Catalysts Supported on CeO₂

The effects of different additives, such as alkaline metal (Cs), alkaline earth metals such as magnesium (Mg), calcium (Ca), and barium (Ba), lanthanum (La), and yttrium (Y), on the performance of Ni/CeO₂ catalysts were studied. Figure 7 shows the ammonia conversion over the reactor temperature for ceria-supported nickel catalysts with different additives.

Doping with cesium (Cs) did not enhance the catalysts performance and even led to a small reduction in ammonia conversion over nearly the entire temperature range. Only at high temperatures of 750 and 800 °C were comparable conversions achieved. A possible explanation for this reduction in activity due to the addition of Cs was the reduced nickel dispersion observed for this catalyst in the H₂ chemisorption data.

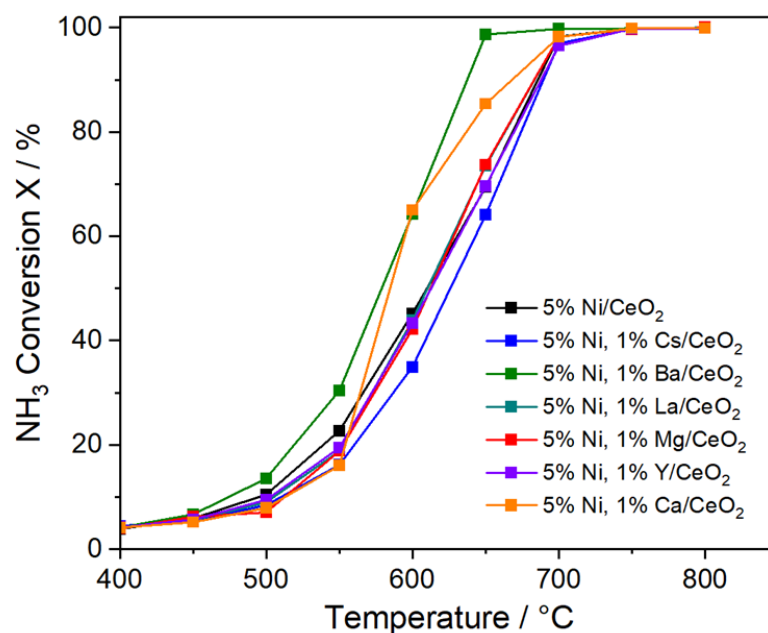


Figure 7. Ammonia conversion over reactor temperature for nickel catalysts supported on CeO₂ with different additives. WHSV = 200 L g_{cat}⁻¹ h⁻¹, 10% Ar, 90% NH₃, and *p* = 5 bar.

The lanthanum-doped catalyst exhibited slightly increased ammonia conversion in the temperature range of 600 to 800 °C compared to that of the non-doped catalyst. At lower temperatures, a small reduction in ammonia conversion was evident in the data. The magnesium-doped catalyst showed a very similar performance to that of the lanthanum-doped catalyst. Again, a small decrease in activity at low temperatures and an increase in activity at higher temperatures was observed for the magnesium-doped catalyst.

The addition of yttrium had almost no effect on the catalytic performance. Only a small reduction in ammonia conversion at lower temperatures was evident. The ammonia conversion at temperatures of 600 °C and higher was similar to that of the Ni/CeO₂ catalyst without a dopant.

The addition of calcium showed a pronounced effect at higher reaction temperatures of 600 °C and higher, where the conversion was significantly increased compared to that of the catalyst without a dopant. At lower temperatures, the addition of calcium did not alter the catalytic performance.

Barium was the best out of the tested additives, as it had increased conversion over the entire temperature range. Especially at higher temperatures, the effect of barium addition was very pronounced. At 600 and 700 °C, the conversion when using the barium-doped catalyst was 35% higher than that observed for the catalyst without a dopant. Furthermore, the barium-doped catalyst surpassed the ammonia conversion of the aforementioned Ru/SiO₂ catalyst at 700 °C and higher. The strong promotive effect of barium on nickel-based catalysts was also previously reported for Ni/Al₂O₃ and Ni/Y₂O₃ catalysts [38].

Kaname Okura et al. studied barium- and strontium-modified nickel catalysts in NH₃-TPSR and detected less strongly adsorbed nitrogen atoms for the modified samples than for a non-modified Ni/Y₂O₃ catalyst. They concluded that this could be attributed to enhancement in the electron density of the nickel due to the interaction with the strong basic barium or strontium promoter [11].

2.2.4. Variations in the Barium Loading of Barium-Promoted Ni/CeO₂ Catalysts

The addition of barium showed the most pronounced improvement in catalytic performance; hence, the effect of barium loading was investigated. The catalysts with 1 and 2% barium showed comparable catalytic performance, which was made evident by the ammonia conversion shown in Figure 8. Only at lower temperatures did the higher

loading of 2% lead to a marginal improvement in ammonia conversion. A further increase in barium loading to 4% led to a decrease in catalytic performance compared to that of the 1 and 2% barium loadings.

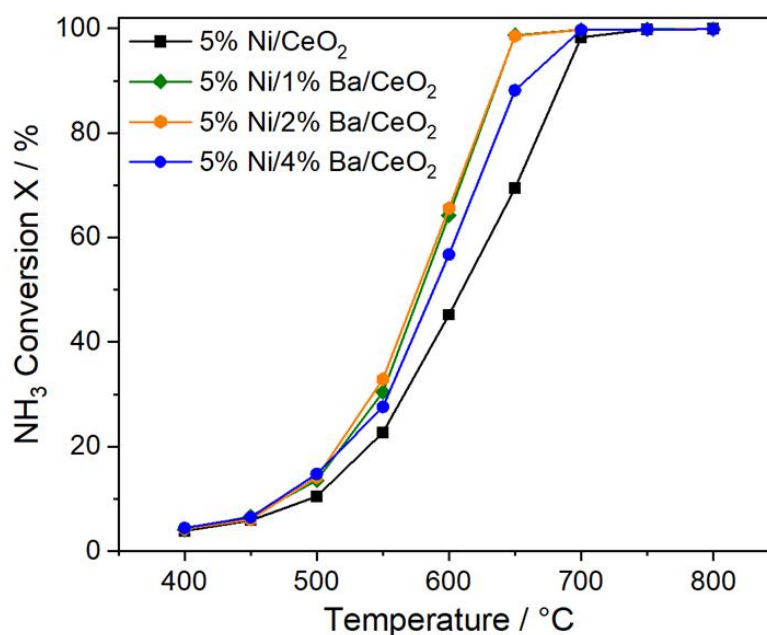


Figure 8. Ammonia conversion over reactor temperature for barium-doped nickel catalysts supported on CeO₂ with different barium loadings. WHSV = 200 L g_{cat}⁻¹ h⁻¹, 10% Ar, 90% NH₃, and *p* = 5 barg.

2.2.5. Variations in the Lanthanum Loading of Lanthanum-Promoted Ni/CeO₂ Catalysts

The effect of the lanthanum loading on the catalytic performance of nickel catalysts supported on CeO₂ was studied (see Figure 9). With the exception of the 1% lanthanum catalyst at low temperatures, increasing the lanthanum loading resulted in increased ammonia conversion. At a reaction temperature of 650 °C, the catalysts doped with 1, 2, and 4% lanthanum reached 73.5, 76.8, and 85.6% ammonia conversion.

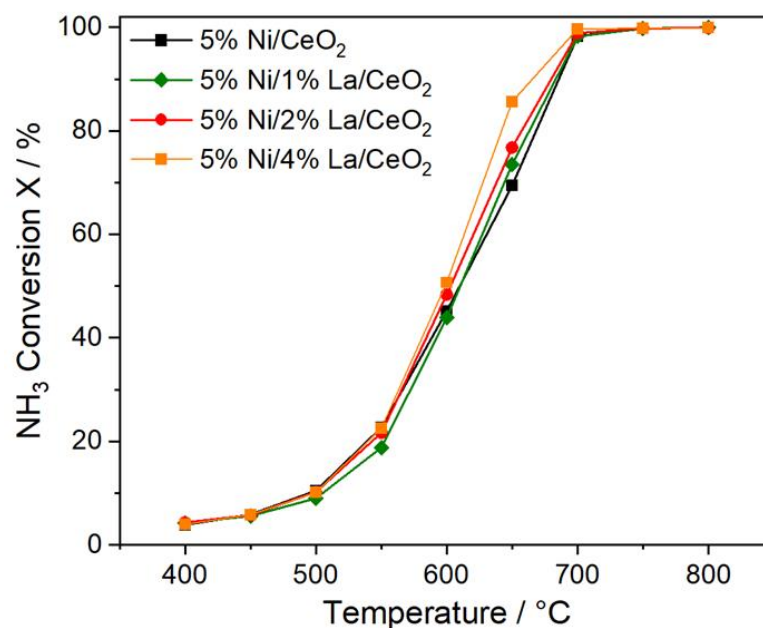


Figure 9. Ammonia conversion over reactor temperature for lanthanum-doped nickel catalysts supported on CeO₂ with different lanthanum loadings. WHSV = 200 L g_{cat}⁻¹ h⁻¹, 10% Ar, 90% NH₃, and *p* = 5 barg.

2.2.6. Long-Term Catalytic Stability

Stability tests were carried out at a reaction temperature of 700 °C for up to 225 h. A Ru/SiO₂ catalyst was compared to a Ni/CeO₂ catalyst. Both catalysts initially showed a stable ammonia conversion rate of over 99.5% (see Figure 10). The ruthenium-based catalyst started to be deactivated and lose activity after about 5.5 h of time on stream. The catalyst deactivation proceeded rapidly, and the ammonia conversion dropped by nearly half after 9 h of time on stream. In the literature, ruthenium catalysts were found to be deactivated by sintering and Ru volatilization at temperatures as low as 450 °C [40]. In contrast, the nickel-based catalyst showed no signs of deactivation, even after 225 h of time on stream at 700 °C.

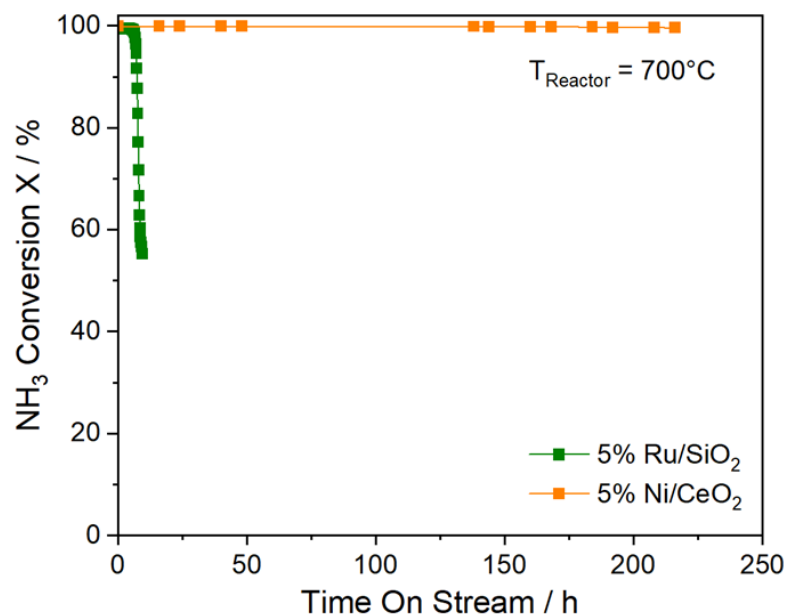


Figure 10. Ammonia conversion over time on stream with nickel (5% Ni, 1% Ba/CeO₂) and ruthenium catalysts. $T_{\text{reactor}} = 700\text{ °C}$, $\text{WHSV} = 200\text{ L g}_{\text{cat}}^{-1}\text{ h}^{-1}$, 10% Ar, 90% NH₃, and $p = 5\text{ barg}$.

3. Discussion

The hydrogen production rates for the tested catalysts at a reactor temperature of 650 °C are shown in Figure 11. The catalysts supported by CeO₂ showed much higher hydrogen production rates than those of the catalysts supported by SiO₂ and Al₂O₃. The highest hydrogen production rates were evident for CeO₂-supported nickel catalysts that were doped with either barium or calcium.

The hydrogen production rates at 600–650 °C achieved in this work were very high compared to values found in the literature, as displayed in Table 2.

The comparison might have been flawed, since the catalysts in this work were applied as coatings, while most studies in the literature tested the catalysts as powders in a fixed-bed reactor. The thin catalyst coatings resulted in much higher catalyst utilization, and microreactors commonly show a much better temperature distribution than that of fixed-bed reactors. Hence, the good performance might have been caused not only by the high activity of the developed catalysts, but also by the advantageous microreactor technology.

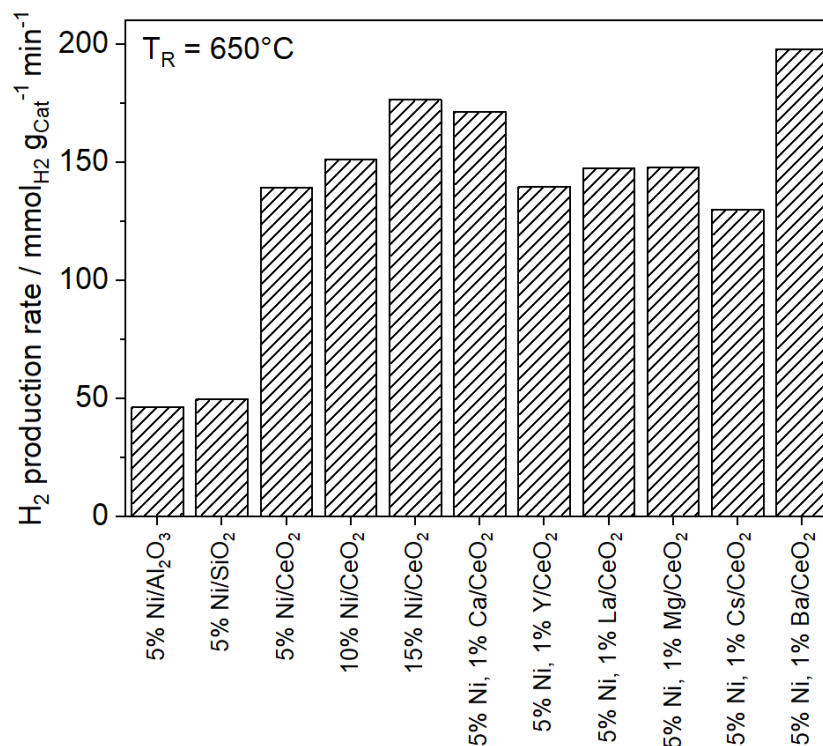


Figure 11. Hydrogen production rates at 650 °C for different catalysts. WHSV = 200 L g_{cat}⁻¹ h⁻¹, 10% Ar, 90% NH₃, and $p = 5$ barg.

Table 2. Comparison of different catalysts for ammonia decomposition.

Catalyst	Temperature °C	NH ₃ Conversion %	H ₂ Production Rate mmol _{H₂} g _{cat} ⁻¹ min ⁻¹
2.8% Cs-Ru/MgO [44]	500	88.2	59.1
5% K-Ru/CNTs [16]	450	97.3	32.6
0.97% Ru/Fe-C [45]	600	97.5	21.7
5% Ru/graphitic C [46]	550	95.0	29.1
9.6% Ru/SiO ₂ [47]	500	86.0	345.5
15% Ni/Mica [48]	650	97.2	32.5
Ni _{0.6} (Mg _{0.29} Al _{0.57} O _n) [49]	600	99.3	33.3
12% Ni/MRM [50]	700	95.5	32.0
Ni ₁ /C-LDH _s -ST [51]	600	98.8	11.0
5% Ni/ZSM [52]	650	97.6	32.7
19.3% Ni/Al ₁ Ce _{0.05} O _x [42]	600	81.8	49.3
5% Ru/SiO ₂ (this work)	650	99.0	198.8
5% Ni, 4% La/CeO ₂ (this work)	650	88.1	176.9
5% Ni, 2% Ba/CeO ₂ (this work)	650	98.5	198.2

4. Materials and Methods

Preparation of catalysts and assembly of microreactors: The microreactor that was used with 14 channels can be seen in Figure 1 (the channel dimensions of the assembled reactor were 500 μm × 500 μm, with a channel length of 25 mm).

Catalyst powder preparation: The first step of the catalyst powder preparation was impregnating the support (Al₂O₃ Puralox, Sasol, SiO₂ Ludox AS-40 (Merck, Darmstadt, Germany) CeO₂ nanopowder, <25 nm, Sigma Aldrich, St. Louis, MO, USA) with an aqueous solution of the metal precursor (Ni(NO₃)₂·6H₂O, Sigma Aldrich or Ru(NO)(NO₃)₃, Alfa Aesar, Haverhill, USA) and the dopant precursor to obtain the desired catalyst composition.

The precursors for the dopants were $\text{Ca}(\text{NO}_3)_2 \times 4\text{H}_2\text{O}$ (Sigma Aldrich), $\text{Y}(\text{NO}_3)_3 \times 6\text{H}_2\text{O}$ (Alfa Aesar), $\text{Ba}(\text{NO}_3)_2$ (Alfa Aesar), $\text{Mg}(\text{NO}_3)_2 \times 6\text{H}_2\text{O}$ (Sigma Aldrich), $\text{La}(\text{NO}_3)_3 \times 6\text{H}_2\text{O}$ (Sigma Aldrich), and CsNO_3 (Sigma Aldrich). The impregnated powders were then calcined at 450 °C for 6 h in an air atmosphere and then milled.

Wash-coating of the catalyst: Details on the wash-coating procedure can be found in our previous work [53]. For the wash-coating, a suspension of the catalyst power, deionized water, polyvinyl alcohol, and acetic acid was used. The microchannels of the reactor plates were filled with the homogeneous catalyst suspension before the excess was removed with a blade, and the plates were dried at room temperature. After drying, the plates were calcined at 450 °C in an air atmosphere.

Two reactor plates coated with the catalyst were sandwiched together and assembled via laser welding to form a microreactor, as described in previous papers [54].

Catalytic testing: Catalytic tests were carried out using a test rig with online analytics. The microreactor was placed in a stainless-steel heating block with two 300 W heating cartridges and different thermocouples. Gaseous ammonia (5.0 purity) and argon were dosed via Bronkhorst mass flow controllers. Then, 10% argon was added as an internal standard for the calculation of the mass balance. All lines were heat-traced.

The pressure was controlled by a back-pressure regulator downstream of the reactor (Equilibar[®] Research Serie LF, Equilibar, Fletscher, United States).

The gas was analyzed online via a Gasmeter FTIR spectrometer (used for the measurement of the ammonia concentration) and an Agilent (Santa Clara, CA, USA) μGC (used for the measurement of hydrogen, nitrogen, and argon concentrations).

Before every experiment, bypass measurements were carried out to measure the feed concentration. The reactors contained between 20 and 25 mg of catalyst. For the catalytic measurements, the flow rates were adjusted according to the catalyst mass (ammonia and argon flow rates of 60–75 and 6.7–8.3 mL/min, respectively) to realize a weight hourly space velocity (WHSV) of 200 L/g_{catalyst} h.

Catalyst characterization: The loadings of the active metals and dopants were analyzed by using XRF spectroscopy (ED-XRF 1510 Canberra Packard Central Europe GmbH, Schwadorf, Austria) equipped with Cd-109 (22 keV) and Am-241 (60 keV) as an electron source).

For the transmission electron microscopy (TEM) measurements, a Libra 120 (Zeiss, Oberkochen, Germany) instrument was used. Nitrogen sorption isotherms were measured at −273 °C on a Autosorb iQ (Anton Paar, Graz, Austria) instrument after degassing the sample at 250 °C for 12 h.

X-ray photoelectron spectroscopy (XPS) investigations were carried out using a multi-chamber UHV system (PREVAC). The spectra were measured using a hemispherical Scienta R4000 electron instrument (Scienta Omicron AB, Uppsala, Sweden) equipped with an Al K α X-ray source (1486.6 eV, 0.8 eV band) and XM 650 X-ray Monochromator (Scienta Omicron AB, Uppsala, Sweden) (0.2 eV band). The pass energies were set to 200 eV and 50 eV for the survey and high-resolution spectra, respectively. The pressures during the measurements were below 3×10^{-8} mbar.

H₂ chemisorption: Measurements were carried out using a Autosorb TPX instrument (Anton Paar, Graz, Austria). Before measurement, the samples were degassed under a helium flow at 120 °C for 30 min and reduced under a pure hydrogen flow at 600 °C for 120 min. After the reduction, the remaining hydrogen was removed through evacuation at 600 °C for one hour. The measurements were conducted at 45 °C. One combined isotherm was measured (strong and weak adsorption); then, the sample was evacuated for 1 h to remove weakly adsorbed hydrogen. Then, another isotherm was measured to obtain the amount of weakly adsorbed hydrogen. The chemisorption isotherm was obtained by subtracting the weak isotherm from the combined isotherm.

5. Conclusions

This study showed that nickel catalysts are promising for the decomposition of ammonia at high temperatures and elevated pressures. The nickel catalysts showed high activity at temperatures over 600 °C, and a doped nickel catalyst surpassed the ammonia conversion rate of a highly active ruthenium catalyst at 650 °C.

Operation at elevated pressure made a higher temperature necessary to achieve the goal of conversion exceeding 99%. At 700 °C, the ruthenium-based catalyst was rapidly deactivated, which disqualified it for high-temperature applications. The nickel catalysts were generally less active than ruthenium but showed a much-improved high-temperature stability. While the nickel-based catalysts were less active, this disadvantage vanished at high temperatures, and the optimized nickel catalyst surpassed the activity of ruthenium at temperatures of 700 °C and higher.

The addition of dopants from the elements in the alkali and earth alkali groups, as well as lanthanum, enhanced activity. However, some elements, such as La, Ca, and Ba, showed a much greater effect. Barium proved to be the best additive and enhanced the activity drastically. The loading of the dopant, affected the catalytic performance differently for barium and lanthanum. Increasing the lanthanum loading showed an increase in performance. The ammonia conversion when using barium-doped catalysts was at its maximum for a loading of 2 wt.% barium.

In conclusion, it can be stated that the combination of excellent catalyst stability, good activity, and low cost makes nickel-based catalysts a promising candidate for ammonia decomposition, especially in decentralized and mobile applications that require high conversion rates.

Further catalyst optimization led to highly stable and active catalyst formulations that were applied to the demonstrator plant (2.9 kg/h hydrogen) developed within the Ammonpaktor project. The results of the operation of this large decomposition unit will be disseminated shortly. The stability of the developed catalyst in the presence of traces of water (0.5%) in the ammonia fed into the decomposition reactor was also studied in the framework of this project and will also be disseminated.

Supplementary Materials: The following supporting information can be downloaded at: <https://www.mdpi.com/article/10.3390/catal14020104/s1>, Table S1: XRF analysis data of the used catalysts; Figure S1: Additional TEM micrographs of nickel-based catalysts supported on Al₂O₃, SiO₂ and CeO₂; Figure S2: EDX mapping of 5%Ni, 1% Cs/CeO₂ catalyst; Figure S3: EDX mapping of 5%Ni, 1% La/CeO₂ catalyst; Figure S4: EDX mapping of 5%Ni, 1% Ba/CeO₂ catalyst; Figure S5: Nitrogen sorption isotherms of the used catalyst supports; Figure S6: Oxygen XPS results for nickel catalysts on different supports; Figure S7: H₂ Chemisorption isotherms of supported nickel catalysts.

Author Contributions: Conceptualization, G.K., H.P., and T.W.; investigation, T.W. and R.Z.; writing—original draft preparation, T.W.; writing—review and editing, T.W., R.Z., H.P., and G.K.; visualization, T.W.; supervision, G.K.; project administration, H.P. and G.K.; funding acquisition, G.K. All authors have read and agreed to the published version of the manuscript.

Funding: Financial support for the AMMONPAKTOR project was provided by the EFRE program of the German region Rhineland-Palatinate under grant no. 84009390.

Data Availability Statement: The data presented in this study are available.

Conflicts of Interest: The authors declare no conflicts of interest.

References

1. Sartbaeva, A.; Kuznetsov, V.L.; Wells, S.A.; Edwards, P.P. Hydrogen nexus in a sustainable energy future. *Energy Environ. Sci.* **2008**, *1*, 79–85. [[CrossRef](#)]
2. Teichmann, D.; Arlt, W.; Wasserscheid, P. Liquid Organic Hydrogen Carriers as an efficient vector for the transport and storage of renewable energy. *Int. J. Hydrogen Energy* **2012**, *37*, 18118–18132. [[CrossRef](#)]
3. Kojima, Y.; Yamaguchi, M. Ammonia as a hydrogen energy carrier. *Int. J. Hydrogen Energy* **2022**, *47*, 22832–22839. [[CrossRef](#)]
4. Lamb, K.E.; Dolan, M.D.; Kennedy, D.F. Ammonia for hydrogen storage; A review of catalytic ammonia decomposition and hydrogen separation and purification. *Int. J. Hydrogen Energy* **2019**, *44*, 3580–3593. [[CrossRef](#)]

5. Ayvalı, T.; Edman Tsang, S.C.; van Vrijaldenhoven, T. The Position of Ammonia in Decarbonising Maritime Industry: An Overview and Perspectives: Part I: Technological advantages and the momentum towards ammonia-propelled shipping. *Johns. Matthey Technol. Rev.* **2021**, *65*, 275–290. [[CrossRef](#)]
6. Shacham, M.; Brauner, N. A hundred years of chemical equilibrium calculations—The case of ammonia synthesis. *Educ. Chem. Eng.* **2015**, *13*, 17–23. [[CrossRef](#)]
7. Di Carlo, A.; Vecchione, L.; Del Prete, Z. Ammonia decomposition over commercial Ru/Al₂O₃ catalyst: An experimental evaluation at different operative pressures and temperatures. *Int. J. Hydrogen Energy* **2014**, *39*, 808–814. [[CrossRef](#)]
8. Mojtahedi, W.; Abbasian, J. Catalytic decomposition of ammonia in a fuel gas at high temperature and pressure. *Fuel* **1995**, *74*, 1698–1703. [[CrossRef](#)]
9. Sayas, S.; Morlanés, N.; Katikaneni, S.P.; Harale, A.; Solami, B.; Gascon, J. High pressure ammonia decomposition on Ru–K/CaO catalysts. *Catal. Sci. Technol.* **2020**, *10*, 5027–5035. [[CrossRef](#)]
10. Ganley, J.C.; Thomas, F.S.; Seebauer, E.G.; Masel, R.I. A Priori Catalytic Activity Correlations: The Difficult Case of Hydrogen Production from Ammonia. *Catal. Lett.* **2004**, *96*, 117–122. [[CrossRef](#)]
11. Okura, K.; Okanishi, T.; Muroyama, H.; Matsui, T.; Eguchi, K. Additive effect of alkaline earth metals on ammonia decomposition reaction over Ni/Y₂O₃ catalysts. *RSC Adv.* **2016**, *6*, 85142–85148. [[CrossRef](#)]
12. Hill, A.K.; Torrente-Murciano, L. Low temperature H₂ production from ammonia using ruthenium-based catalysts: Synergetic effect of promoter and support. *Appl. Catal. B Environ.* **2015**, *172–173*, 129–135. [[CrossRef](#)]
13. Hu, X.-C.; Fu, X.-P.; Wang, W.-W.; Wang, X.; Wu, K.; Si, R.; Ma, C.; Jia, C.-J.; Yan, C.-H. Ceria-supported ruthenium clusters transforming from isolated single atoms for hydrogen production via decomposition of ammonia. *Appl. Catal. B Environ.* **2020**, *268*, 118424. [[CrossRef](#)]
14. Li, X.-K.; Ji, W.-J.; Zhao, J.; Wang, S.-J.; Au, C.-T. Ammonia decomposition over Ru and Ni catalysts supported on fumed SiO₂, MCM-41, and SBA-15. *J. Catal.* **2005**, *236*, 181–189. [[CrossRef](#)]
15. Nagaoka, K.; Eboshi, T.; Abe, N.; Miyahara, S.-I.; Honda, K.; Sato, K. Influence of basic dopants on the activity of Ru/Pr₆O₁₁ for hydrogen production by ammonia decomposition. *Int. J. Hydrogen Energy* **2014**, *39*, 20731–20735. [[CrossRef](#)]
16. Yin, S.-F.; Xu, B.-Q.; Ng, C.-F.; Au, C.-T. Nano Ru/CNTs: A highly active and stable catalyst for the generation of CO_x-free hydrogen in ammonia decomposition. *Appl. Catal. B Environ.* **2004**, *48*, 237–241. [[CrossRef](#)]
17. Yin, S.-F.; Zhang, Q.-H.; Xu, B.-Q.; Zhu, W.-X.; Ng, C.-F.; Au, C.-T. Investigation on the catalysis of CO_x-free hydrogen generation from ammonia. *J. Catal.* **2004**, *224*, 384–396. [[CrossRef](#)]
18. Kim, H.B.; Park, E.D. Ammonia decomposition over Ru catalysts supported on alumina with different crystalline phases. *Catal. Today* **2023**, *411–412*, 113817. [[CrossRef](#)]
19. Cao, C.-F.; Wu, K.; Zhou, C.; Yao, Y.-H.; Luo, Y.; Chen, C.-Q.; Lin, L.; Jiang, L. Electronic metal-support interaction enhanced ammonia decomposition efficiency of perovskite oxide supported ruthenium. *Chem. Eng. Sci.* **2022**, *257*, 117719. [[CrossRef](#)]
20. García-García, F.R.; Guerrero-Ruiz, A.; Rodríguez-Ramos, I.; Goguet, A.; Shekhtman, S.O.; Hardacre, C. TAP studies of ammonia decomposition over Ru and Ir catalysts. *Phys. Chem. Chem. Phys.* **2011**, *13*, 12892–12899. [[CrossRef](#)]
21. Raróg-Pilecka, W.; Szmigielski, D.; Kowalczyk, Z.; Jodzis, S.; Zielinski, J. Ammonia decomposition over the carbon-based ruthenium catalyst promoted with barium or cesium. *J. Catal.* **2003**, *218*, 465–469. [[CrossRef](#)]
22. Yin, S.F.; Xu, B.Q.; Wang, S.J.; Ng, C.F.; Au, C.T. Magnesia–Carbon Nanotubes (MgO–CNTs) Nanocomposite: Novel Support of Ru Catalyst for the Generation of CO_x-Free Hydrogen from Ammonia. *Catal. Lett.* **2004**, *96*, 113–116. [[CrossRef](#)]
23. Yin, S.F.; Xu, B.Q.; Zhu, W.X.; Ng, C.F.; Zhou, X.P.; Au, C.T. Carbon nanotubes-supported Ru catalyst for the generation of CO_x-free hydrogen from ammonia. *Catal. Today* **2004**, *93–95*, 27–38. [[CrossRef](#)]
24. Osozawa, M.; Hori, A.; Fukai, K.; Honma, T.; Oshima, K.; Satokawa, S. Improvement in ammonia synthesis activity on ruthenium catalyst using ceria support modified a large amount of cesium promoter. *Int. J. Hydrogen Energy* **2022**, *47*, 2433–2441. [[CrossRef](#)]
25. Nuss, P.; Eckelman, M.J. Life Cycle Assessment of Metals: A Scientific Synthesis. *PLoS ONE* **2014**, *9*, e101298. [[CrossRef](#)]
26. Lucentini, I.; Garcia, X.; Vendrell, X.; Llorca, J. Review of the decomposition of ammonia to generate hydrogen. *Ind. Eng. Chem. Res.* **2021**, *60*, 18560–18611. [[CrossRef](#)]
27. Muroyama, H.; Saburi, C.; Matsui, T.; Eguchi, K. Ammonia decomposition over Ni/La₂O₃ catalyst for on-site generation of hydrogen. *Appl. Catal. A Gen.* **2012**, *443–444*, 119–124. [[CrossRef](#)]
28. Okura, K.; Okanishi, T.; Muroyama, H.; Matsui, T.; Eguchi, K. Ammonia Decomposition over Nickel Catalysts Supported on Rare-Earth Oxides for the On-Site Generation of Hydrogen. *ChemCatChem* **2016**, *8*, 2988–2995. [[CrossRef](#)]
29. Podila, S.; Al-Zahrani, A.A.; Pasupulety, N.; Alamoudi, M.A. Influence of CaCe ratio on the hydrogen production from ammonia over CaO–CeO₂ supported Co catalysts. *Arab. J. Chem.* **2023**, *16*, 105235. [[CrossRef](#)]
30. Cho, E.H.; Jeon, N.; Yoon, B.S.; Kim, S.; Yun, Y.; Ko, C.H. Magnesium-promoted Ni/USY catalysts prepared via surfactant-assisted melt infiltration for ammonia decomposition. *Appl. Surf. Sci.* **2023**, *608*, 155244. [[CrossRef](#)]
31. Podila, S.; Driss, H.; Ali, A.M.; Al-Zahrani, A.A.; Daous, M.A. Influence of Ce substitution in LaMO₃ (M = Co/Ni) perovskites for CO_x-free hydrogen production from ammonia decomposition. *Arab. J. Chem.* **2022**, *15*, 103547. [[CrossRef](#)]
32. Gu, Y.; Ma, Y.; Long, Z.; Zhao, S.; Wang, Y.; Zhang, W. One-pot synthesis of supported Ni@Al₂O₃ catalysts with uniform small-sized Ni for hydrogen generation via ammonia decomposition. *Int. J. Hydrogen Energy* **2021**, *46*, 4045–4054. [[CrossRef](#)]

33. Zhang, H.; Alhamed, Y.A.; Kojima, Y.; Al-Zahrani, A.A.; Miyaoka, H.; Petrov, L.A. Structure and catalytic properties of Ni/MWCNTs and Ni/AC catalysts for hydrogen production via ammonia decomposition. *Int. J. Hydrogen Energy* **2014**, *39*, 277–287. [[CrossRef](#)]
34. Im, Y.; Muroyama, H.; Matsui, T.; Eguchi, K. Ammonia decomposition over nickel catalysts supported on alkaline earth metal aluminate for H₂ production. *Int. J. Hydrogen Energy* **2020**, *45*, 26979–26988. [[CrossRef](#)]
35. Liu, H.; Wang, H.; Shen, J.; Sun, Y.; Liu, Z. Promotion effect of cerium and lanthanum oxides on Ni/SBA-15 catalyst for ammonia decomposition. *Catal. Today* **2008**, *131*, 444–449. [[CrossRef](#)]
36. Zhang, J.; Xu, H.; Jin, X.; Ge, Q.; Li, W. Characterizations and activities of the nano-sized Ni/Al₂O₃ and Ni/La–Al₂O₃ catalysts for NH₃ decomposition. *Appl. Catal. A Gen.* **2005**, *290*, 87–96. [[CrossRef](#)]
37. Zhang, J.; Xu, H.; Li, W. Kinetic study of NH₃ decomposition over Ni nanoparticles: The role of La promoter, structure sensitivity and compensation effect. *Appl. Catal. A Gen.* **2005**, *296*, 257–267. [[CrossRef](#)]
38. Zheng, W.; Zhang, J.; Ge, Q.; Xu, H.; Li, W. Effects of CeO₂ addition on Ni/Al₂O₃ catalysts for the reaction of ammonia decomposition to hydrogen. *Appl. Catal. B Environ.* **2008**, *80*, 98–105. [[CrossRef](#)]
39. Biesinger, M.C.; Payne, B.P.; Lau, L.W.M.; Gerson, A.; Smart, R.S.C. X-ray photoelectron spectroscopic chemical state quantification of mixed nickel metal, oxide and hydroxide systems. *Surf. Interface Anal.* **2009**, *41*, 324–332. [[CrossRef](#)]
40. Lucentini, I.; Casanovas, A.; Llorca, J. Catalytic ammonia decomposition for hydrogen production on Ni, Ru and NiRu supported on CeO₂. *Int. J. Hydrogen Energy* **2019**, *44*, 12693–12707. [[CrossRef](#)]
41. Li, Y.; Zhang, W.; Ren, J.; Zhou, W.; Wang, Z. Ammonia decomposition for carbon-free hydrogen production over Ni/Al–Ce catalysts: Synergistic effect between Al and Ce. *Fuel* **2024**, *358*, 130176. [[CrossRef](#)]
42. Do, Q.C.; Kim, Y.; Le, T.A.; Kim, G.J.; Kim, J.-R.; Kim, T.-W.; Lee, Y.-J.; Chae, H.-J. Facile one-pot synthesis of Ni-based catalysts by cation-anion double hydrolysis method as highly active Ru-free catalysts for green H₂ production via NH₃ decomposition. *Appl. Catal. B Environ.* **2022**, *307*, 121167. [[CrossRef](#)]
43. Huang, C.; Yu, Y.; Tang, X.; Liu, Z.; Zhang, J.; Ye, C.; Ye, Y.; Zhang, R. Hydrogen generation by ammonia decomposition over Co/CeO₂ catalyst: Influence of support morphologies. *Appl. Surf. Sci.* **2020**, *532*, 147335. [[CrossRef](#)]
44. Zhang, J.; Xu, H.; Ge, Q.; Li, W. Highly efficient Ru/MgO catalysts for NH₃ decomposition: Synthesis, characterization and promoter effect. *Catal. Commun.* **2006**, *7*, 148–152. [[CrossRef](#)]
45. Li, L.; Chen, F.; Dai, Y.; Wu, J.; Shao, J.L.; Li, H.Y. Fe-assisted Ru clusters supported on porous and graphitic carbon for ammonia decomposition to CO_x free hydrogen. *RSC Adv.* **2016**, *6*, 102336–102342. [[CrossRef](#)]
46. Li, L.; Zhu, Z.H.; Yan, Z.F.; Lu, G.Q.; Rintoul, L. Catalytic ammonia decomposition over Ru/carbon catalysts: The importance of the structure of carbon support. *Appl. Catal. A Gen.* **2007**, *320*, 166–172. [[CrossRef](#)]
47. Varisli, D.; Elverisli, E.E. Synthesizing hydrogen from ammonia over Ru incorporated SiO₂ type nanocomposite catalysts. *Int. J. Hydrogen Energy* **2014**, *39*, 10399–10408. [[CrossRef](#)]
48. Hu, Z.-P.; Weng, C.-C.; Yuan, G.-G.; Lv, X.-W.; Yuan, Z.-Y. Ni nanoparticles supported on mica for efficient decomposition of ammonia to CO_x-free hydrogen. *Int. J. Hydrogen Energy* **2018**, *43*, 9663–9676. [[CrossRef](#)]
49. Su, Q.; Gu, L.; Yao, Y.; Zhao, J.; Ji, W.; Ding, W.; Au, C.-T. Layered double hydroxides derived Ni_x(Mg_yAl_zO_n) catalysts: Enhanced ammonia decomposition by hydrogen spillover effect. *Appl. Catal. B Environ.* **2017**, *201*, 451–460. [[CrossRef](#)]
50. Cao, J.-L.; Yan, Z.-L.; Deng, Q.-F.; Wang, Y.; Yuan, Z.-Y.; Sun, G.; Jia, T.-K.; Wang, X.-D.; Bala, H.; Zhang, Z.-Y. Mesoporous modified-red-mud supported Ni catalysts for ammonia decomposition to hydrogen. *Int. J. Hydrogen Energy* **2014**, *39*, 5747–5755. [[CrossRef](#)]
51. Zhao, J.; Deng, L.; Zheng, W.; Xu, S.; Yu, Q.; Qiu, X. Nickel-induced structure transformation in hydrocalumite for enhanced ammonia decomposition. *Int. J. Hydrogen Energy* **2020**, *45*, 12244–12255. [[CrossRef](#)]
52. Hu, Z.-P.; Weng, C.-C.; Chen, C.; Yuan, Z.-Y. Catalytic decomposition of ammonia to CO_x-free hydrogen over Ni/ZSM-5 catalysts: A comparative study of the preparation methods. *Appl. Catal. A Gen.* **2018**, *562*, 49–57. [[CrossRef](#)]
53. Zapf, R.; Becker-Willinger, C.; Berresheim, K.; Bolz, H.; Gnaser, H.; Hessel, V.; Kolb, G.; Löb, P.; Pannwitt, A.-K.; Ziogas, A. Detailed characterization of various porous alumina-based catalyst coatings within microchannels and their testing for methanol steam reforming. *Chem. Eng. Res. Des.* **2003**, *81*, 721–729. [[CrossRef](#)]
54. Kolb, G.; Zapf, R.; Hessel, V.; Löwe, H. Propane steam reforming in micro-channels—Results from catalyst screening and optimisation. *Appl. Catal. A Gen.* **2004**, *277*, 155–166. [[CrossRef](#)]

Disclaimer/Publisher’s Note: The statements, opinions and data contained in all publications are solely those of the individual author(s) and contributor(s) and not of MDPI and/or the editor(s). MDPI and/or the editor(s) disclaim responsibility for any injury to people or property resulting from any ideas, methods, instructions or products referred to in the content.